Article

Discovery Medicine 2025; 37(198): 1372–1384
https://doi.org/10.24976/Discov.Med.202537198.119

Bone Marrow Mesenchymal Stem Cells Inhibit Ferroptosis Through Mitochondrial Transfer and Improve Endothelial Cell Dysfunction

Guangkuo Wang[1], Shangqian Li[1], Fang Li[1], Zhigang Zhang[1,*]

[1]Department of Cardiovascular Surgery, Jiangmen Central Hospital, 529000 Jiangmen, Guangdong, China
*Correspondence: zhang999zg@126.com (Zhigang Zhang)
Published: 20 July 2025

Background: Ferroptosis, an iron-dependent form of cell death driven by lipid peroxidation, contributes to endothelial dysfunction and the progression of atherosclerosis. Moreover, mitochondrial damage leads to ferroptosis through accumulation of reactive oxygen species (ROS). This study aimed to determine whether bone marrow mesenchymal stem cells (BMSCs) protect endothelial cells from ferroptosis through mitochondrial transfer.

Methods: Human umbilical vein endothelial cells (HUVECs) were treated with oxidized low-density lipoprotein (ox-LDL) to induce dysfunction. BMSCs were co-cultured with these damaged HUVECs in a direct system without Transwell inserts. Mitochondrial transfer was evaluated using MitoTracker probes. Key indicators, including adenosine triphosphate (ATP) production, mitochondrial membrane potential, ferroptosis markers (Fe^{2+}, ROS, malondialdehyde (MDA), lactate dehydrogenase (LDH)), and ferroptosis-related protein expression (Glutathione Peroxidase 4 (GPX4), Solute Carrier Family 7 Member 11(SLC7A11), Acyl-CoA Synthetase Long Chain Family Member 4 (ACSL4)) were assessed. Furthermore, rescue experiments were performed using ferroptosis activator Rat Sarcoma Viral Oncogene Homolog (RAS)-selective lethal small molecule 3 (RSL3) to validate the underlying mechanisms.

Results: Dual fluorescence microscopy revealed that BMSCs successfully transferred mitochondria to ox-LDL-injured HUVECs. Mitochondrial transfer significantly increased ATP production (1.9-fold, $p < 0.01$), restored mitochondrial membrane potential ($p < 0.01$), and enhanced endothelial viability ($p < 0.01$). Furthermore, ferroptosis-related markers were significantly altered: Fe^{2+}, MDA, LDH, and ROS levels decreased ($p < 0.05$), while glutathione (GSH) levels and anti-ferroptosis protein GPX4 and SLC7A11 increased ($p < 0.01$), and pro-ferroptosis protein ACSL4 decreased ($p < 0.01$). RSL3 treatment reversed these protective effects, confirming the role of ferroptosis inhibition.

Conclusion: This study demonstrates that BMSCs can inhibit ferroptosis and restore endothelial cell function via mitochondrial transfer. These findings offer novel therapeutic insights into the treatment of atherosclerosis by targeting ferroptosis.

Keywords: atherosclerosis; ferroptosis; BMSCs; mitochondria; endothelial function

Introduction

Atherosclerosis (AS) is a chronic inflammatory disease associated with an increased risk of cardiovascular and cerebrovascular disorders, including thrombosis, chronic lumen stenosis, and plaque rupture [1]. In recent years, the incidence of AS has reportedly increased, posing a significant risk to public health and life expectancy [2]. Despite technological advancements, the precise pathogenesis of AS remains unexplored. Current evidence indicates that AS is a chronic vascular inflammation induced by the interaction of arterial wall cells with detrimental factors such as smoking, diabetes, hypertension, and other risk contributors [3]. The endothelium, which forms the innermost layer of blood arteries, plays a crucial role, and its dysfunction is widely recognized as an early predictor of AS [4]. Activation of endothelial cells and the secretion of cytokines by macrophages trigger vascular smooth muscle cells to produce fibromuscular plaques. As complex plaques form, the endothelial cells adopt a pro-inflammatory phenotype regulated by inflammatory cell populations, leading to plaque structural instability and eventual rupture [5]. Therefore, alleviating endothelial cell dysfunction to prevent the malignant development of AS has become a significant focus of current research.

Iron plays a crucial role in fundamental life processes, and an imbalance between its intake and output can lead to the development of various diseases. Excessive levels of free iron within cells accelerate the oxidation of low-density lipoprotein (LDL), which is subsequently absorbed by the LDL receptor on macrophages, resulting in the production of foam cells and the progression of AS [6]. Ferroptosis, a recently identified form of iron-dependent cell death, is associated with iron overload, accumulation of re-

active oxygen species, lipid peroxidation, and glutamate build-up, and is now considered one of the mechanisms contributing to endothelial dysfunction [7]. According to Bai *et al.* [8], inhibiting ferroptosis can lower lipid peroxidation and endothelial cell dysfunction, thereby alleviating AS progression. Nevertheless, approaches to prevent ferroptosis in endothelial cells remain to be investigated. Moreover, mitochondrial damage or dysfunction can induce excessive reactive oxygen species (ROS)-mediated oxidative stress, which in turn causes ferroptosis, underscoring the close association between ferroptosis and mitochondrial function [9]. Therefore, maintaining mitochondrial functional homeostasis may represent an effective approach to inhibit endothelial cell ferroptosis.

A study has demonstrated the role of mitochondrial damage and dysfunction in the pathophysiology of AS [10]. The transfer of mitochondria between cells has been identified as a key mechanism in tissue repair. Notably, Zhang *et al*. [11] (2023) first confirmed this phenomenon in alveolar epithelial cells during lung injury, while Paliwal *et al*. [12] (2018) reported a comprehensive review of the regenerative functions of mesenchymal stem cells (MSCs) in this context. In endothelial cells, mitochondrial dysfunction can generate excessive reactive oxygen species (ROS), inducing oxidative stress, lipid peroxidation, and ultimately cell death, processes that are key drivers in the initiation and progression of AS [13]. Given this, restoring mitochondrial function is emerging as a potential therapeutic target to alleviate endothelial dysfunction associated with AS.

While mitochondria are responsible for cellular oxygen intake, endothelial cells play a crucial role in transporting oxygen from the pulmonary circulation to the surrounding vascular tissues. In recent years, a growing body of evidence has shown that cells can exchange mitochondria to mitigate oxidative injury. Intercellular mitochondrial transfer, a process in which healthy mitochondria are transferred from functional donor cells to stressed or damaged recipient cells, has been identified as a novel mechanism of cellular repair in various pathological conditions [14]. This transfer increases mitochondrial content and functional capacity of recipient cells, enabling them to resume energy metabolism and maintain redox homeostasis.

The ability of MSCs to donate normal mitochondria has been identified as an emerging strategy for repairing damaged cells or tissues [12]. For example, Li *et al*. [15] confirmed that mitochondrial transfer from bone marrow mesenchymal stem cells (BMSCs) to damaged neurons can provide neuroprotection in spinal cord injury. Among the various MSC subtypes, BMSCs have received particular attention due to their accessibility, strong self-renewal ability, and well-documented efficiency in mitochondrial donation. Their ability to regulate immune responses and secrete trophic factors further enhances their reparative functions, making them especially suitable for targeting vascular and metabolic disorders. BMSCs, which are primitive progenitor cells derived from the mesoderm with self-renewal and potential multi-directional differentiation, are often used as mitochondrial donor cells [16]. Furthermore, the therapeutic potential of BMSCs in treating AS has also been affirmed [16]. However, although mitochondrial transfer has been studied in models of neurological and pulmonary diseases, its role in endothelial dysfunction during atherosclerosis, particularly in preventing ferroptosis, remains yet to be elucidated.

Thus, elucidating whether BMSCs can transfer mitochondria to protect endothelial cells from ferroptosis may provide valuable insight into developing novel anti-atherosclerotic therapies. Against this background, mitochondrial transfer appears to be an effective strategy for protecting against endothelial cell injury. Hence, the present study aimed to explore the mechanism by which BMSCs transfer mitochondria to endothelial cells to inhibit ferroptosis and to further examine how this mechanism impacts endothelial dysfunction. The findings are anticipated to provide a theoretical basis for developing therapeutic strategies to reduce atherosclerotic plaque formation and reduce the progression of AS.

Materials and Methods

Cell Culture and Treatment

Human umbilical vein endothelial cells (HUVECs, Cat# CP-H082) and bone marrow mesenchymal stem cells (BMSCs, Cat# CP-H166) were obtained from Procell Life Science & Technology Co., Ltd. (Procell, Wuhan, China). Both cell lines were authenticated by short tandem repeat (STR) profiling and examined for mycoplasma contamination before use. The cells were cultured in their respective complete media (Procell, Wuhan, China) containing 10% fetal bovine serum (Excell Bio, Shanghai, China), 100 units/mL penicillin, and 50 units/mL streptomycin (Beyotime, Suzhou, China) at 37 °C in the presence of 5% CO_2.

To induce endothelial dysfunction, HUVECs were treated with oxidized low-density lipoprotein (ox-LDL, Solarbio, Beijing, China) at final concentrations of 50 μg/mL and 100 μg/mL for 48 hours. Based on preliminary results, 100 μg/mL ox-LDL was selected as the standard condition for establishing endothelial injury in subsequent co-culture assays.

The direct co-culture system was established by seeding BMSCs and ox-LDL-injured HUVECs in the same well at a ratio of 1:2 cells without a Transwell insert. BMSCs were seeded at a density of 5000 cells/cm^2 and HUVECs at 10,000 cells/cm^2. After inoculation, cells were co-cultured in shared growth medium with medium changes every 2 days.

To evaluate the role of ferroptosis, the specific ferroptosis inducer Rat Sarcoma Viral Oncogene Homolog (RAS)-selective lethal small molecule 3 (RSL3) (Selleck Chemicals, Houston, TX, USA) was used in rescue exper-

iments. RSL3 was dissolved in DMSO and added to the co-culture system at a final concentration of 5 µmol/L for 24 hours. The final DMSO concentration was maintained below 0.1% to avoid solvent-induced cytotoxicity.

Identification of Surface Antigens of BMSCs

The expression levels of surface markers cluster of differentiation 44 (CD44) and cluster of differentiation 45 (CD45) in BMSCs were assessed using flow cytometry. BMSCs in the logarithmic growth phase were seeded at a density of 1×10^6 cells per well on a 6-well plate and incubated for 48 hours. Following digestion, the cells were centrifuged at 800 rpm for five minutes. The cell pellet was thoroughly washed with PBS, centrifuged again, and counted. After that, a 50 µL single-cell suspension was treated with 10 µL of fluorochrome-conjugated antibodies (anti-CD44-FITC, Cat# ab30405, Abcam, Cambridge, UK; and anti-CD45-PE, Cat# ab269297, Abcam, Cambridge, UK) for 60 minutes at room temperature in the dark. Following staining, cells were washed twice with PBS and centrifuged. Finally, the cells were resuspended in PBS before flow cytometric analysis. The results were examined and analyzed using FlowJo software (Version 10.8.1, BD Biosciences, Ashland, OR, USA).

Alizarin Red Staining for Osteogenic Differentiation

BMSCs were inoculated at a density of 5000 cells/cm^2 onto a 24-well plate. After allowing the cells to adhere to the wall for 24 hours, osteogenic induction medium (complete medium + 50 µg/mL Vitamin C + 10 mmol/L β-Sodium glycerophosphate + 100 nmol/L dexamethasone, Beyotime, Suzhou, China) was added. The medium was changed every 2–3 days, and the cells were cultivated for 14 days. After induction, the wells were washed with PBS and fixed with 4% paraformaldehyde (Beyotime, Suzhou, China) at room temperature for 15 minutes. Then, the cells were washed three times with PBS, and stained with Alizarin Red solution (Beyotime, Suzhou, China) for 30 minutes at room temperature. After staining, the formation of calcium nodules in the mineralized matrix was determined based on the intensity and extent of red coloration.

For quantitative analysis, microscopic images were captured from at least five random fields per well under consistent light exposure conditions. The staining intensity was analyzed using ImageJ software (version 1.53t, National Institutes of Health, Bethesda, MD, USA), and results were expressed as mean gray value or integrated density to quantify calcium deposition.

Oil Red O Staining for Lipid Differentiation

After adherence to the wall as stated above, BMSCs were cultured in adipogenic induction medium (complete medium + 1 µg/mL insulin + 10 µmol/L rosiglitazone + 250 nmol/L dexamethasone, Beyotime, Suzhou, China) for 14 days, with the medium changed every 2–3 days. After induction, the cells were fixed with 4% paraformaldehyde (Beyotime, Suzhou, China) and washed with PBS. Oil Red O staining solution (Beyotime, Suzhou, China) was then added, and the cells were stained at room temperature in the dark for 30 minutes. The formation of lipid droplets was determined based on the intensity and extent of red staining.

The stained areas were visualized under a microscope, and ImageJ software was used to quantify the red staining area, and its intensity was determined. Results were expressed as a percentage of the stained area or as integrated density values.

Alcian Blue Staining for Cartilage Differentiation

After adhering to the plate wall according to the above method, BMSCs were cultured in chondrogenic induction medium (complete medium + 0.1 µmol/L dexamethason + 50 µg/mL ascorbic acid + 0.9 mmol/L sodium pyruvate + 1% ITS + 50 µg/mL proline, Beyotime, Suzhou, China) for 14 days, with medium was changes every 2–3 days. After that, the cells were washed and fixed, and then treated with Alcian blue acidification solution (Beyotime, Suzhou, China) for 3 minutes. Subsequently, the cells were stained with Alcian blue staining solution (Beyotime, Suzhou, China) for 30 minutes. Cartilage differentiation was evaluated based on the extent of blue cytoplasmic staining.

For quantitative assessment, stained cells were imaged under consistent conditions, and the blue-stained area was analyzed using ImageJ software to measure integrated optical density (IOD).

The Detection of Cell Apoptosis

The apoptosis rate of HUVECs was determined using the Annexin V-FITC kit (Beyotime, Suzhou, China). Once the cells reached confluence in the monolayer flask, they were detached using 0.25% trypsin-EDTA (Gibco, Waltham, MA, USA), centrifuged, and then resuspended at 1000 rpm for 5 minutes. The cell pellet was then resuspended in pre-made 1X Annexin V binding solution to a final concentration of 1×10^6 cells/mL. After that, 5 µL of Annexin V-FITC complex and 5 µL of PI Solution were added to 100 µL of cell suspension, incubated for 15 minutes at room temperature in the dark. In the next step, 1X Annexin V Binding Solution (400 µL) was added. Finally, the samples were analyzed within one hour using Attune NxT flow cytometry (Invitrogen, Waltham, MA, USA), and data were examined using FlowJo software (Version 10.8.1, BD Biosciences, Ashland, OR, USA).

ELISA Assay

The enzyme-linked immunosorbent assay (ELISA) assay was performed to identify the presence of inflammatory factors. After treatment, the supernatant from each cell group was obtained. Following the manufacturer's instructions (HNYBIO, Shanghai, China), standard curves were

developed, and the expression levels of interleukin-6 (IL-6), tumor necrosis factor-alpha (TNF-α), and interleukin-1 beta (IL-1β) were assessed using an RT-6000 microplate reader (Rayto, Shenzhen, China).

Endothelial Cell Infiltration Assay

The HUVECs cell suspension was adjusted to a concentration of 1×10^5 cells/mL and inoculated into a Transwell chamber insert placed in a 24-well cell culture plate. Before seeding, 1 mL of complete cell culture medium was added to the lower chamber of the culture plate. After incubation and two PBS washes, the Transwell insert was shifted to a fresh 24-well plate. The lower chamber was filled with 600 µL 4% BSA solution, while the upper chamber was filled with 100 µL EB-BSA working solution (MeRCK, Rahway, NJ, USA), ensuring equal liquid levels to prevent leakage due to level differences. The system was equilibrated for 1 hour at 37 °C in a 5% CO_2 cell culture incubator.

After incubation, the Transwell chamber was removed, and the solution from the lower chamber was aspirated and centrifuged at 1000 rpm for 5 minutes. The supernatant was added to a 96-well plate. The EB-BSA working solution (at an initial concentration of 0.67 mg/mL) was serially diluted to develop a standard curve. The OD was measured at 620 nm using an RT-6000 microplate reader (Rayto, Shenzhen, China). Finally, the concentration of EB in the lower Transwell chamber was calculated based on the standard curve to determine the permeability of the endothelial cell monolayer.

Observation of Mitochondrial Transfer

To trace mitochondrial localization, two fluorescent probes were used. BMSCs were stained with MitoTracker Red staining solution (Beyotime, Suzhou, China), and HUVECs were stained with MitoTracker Green (Beyotime, Suzhou, China). Each staining step lasted for 30 minutes at 37 °C. After staining, the solutions were removed and replaced with fresh pre-warmed cell culture medium. Finally, cell nuclei were counterstained with DAPI for 3 minutes. The results were observed and images were recorded using an EVOS M5000 fluorescence microscope (Thermo Fisher, Waltham, MA, USA).

Measurement of Mitochondrial Membrane Potential

Logarithmic-phase HUEVCs were inoculated at a density of 1×10^6 cells per well in a 6-well plate. After washing, 1 mL of diluted TMRE staining solution (Beyotime, Suzhou, China) was added to each well and incubated at 37 °C for 30 minutes. After incubation, the cells were washed twice with preheated cell culture medium. Fluorescence was observed, and images were recorded using an EVOS M5000 fluorescence microscope (Thermo Fisher, Waltham, MA, USA) at a wavelength of 575 nm. The fluorescence intensity was quantified using ImageJ software.

Detection of ATP Levels

The intracellular adenosine triphosphate (ATP) levels were determined using a colorimetric approach. Following the manufacturer's instructions (Njjcbio, Nanjing, China), the appropriate reagents were prepared, and absorbance (A) values were assessed using an RT-6000 microplate reader (Rayto, Shenzhen, China). ATP levels were calculated using the following formula: ATP content (µmol/g prot) = (A determination – A control) / (A standard – A blank) × c standard × N / cpr.

CCK-8 Assay

Cell proliferation capability was examined using the CCK-8 assay (Bioss, Beijing, China). Logarithmic phase cells were collected, counted, and adjusted to the required concentration. After that, 2×10^3 cells/well were seeded into a 96-well plate. After a 12-hour pre-incubation, 10 µL of CCK-8 reagent was added to each well, and the plate was incubated for an additional 2 hours at 37 °C. Absorbance was then measured at 450 nm using an RT-6000 microplate reader (Rayto, Shenzhen, China). Cell proliferation was expressed as cell survival rate, calculated as follows: Cell survival rate (%) = (OD value (sample) – OD value (CCK-8)) / (OD value (control group) – OD value (CCK-8)) × 100%.

Transwell Assay

A Transwell chamber pre-coated with Matrigel was filled with a suspension of HUVECs at a density of 1–5 $\times 10^5$ cells/mL. The lower chamber was filled with 600 µL of culture media containing 10% FBS. The chambers were incubated at 37 °C for 24 hours in a 5% CO_2 incubator to allow cell invasion through the membrane. After that, the cells were washed with PBS and fixed with 4% paraformaldehyde for 10 minutes. The fixative in the bottom chamber was then discarded, the top chamber was removed and stained with crystal violet staining solution (Sigma-Aldrich, St. Louis, MO, USA) for 10 minutes. Following staining, the insert was thoroughly washed with water and air-dried. Finally, invasion cells were assessed using a microscope.

Wound Healing Assay

HUVECs were seeded in a 6-well plate at a density of 1×10^6 cells/well and incubated for 4 hours. After cells adhered to the plate wall, drug treatment was applied as required. Once the cell achieved over 90% confluence, a straight scratch was made using a sterilized pipette tip along a guideline marked on the back of the plate. The scratch area at 0 hours was observed and imaged under a microscope. The same area was re-observed and imaged after 24 hours to evaluate cell migration.

Detection of Fe^{2+}, GSH, LDH, and MDA Content

The content of ferroptosis-related indicators was assessed using the reagent kit (Beyotime, Suzhou, China) following the manufacturer's instructions. Absorbance was recorded at 593 nm for Fe^{2+}, 412 nm for glutathione (GSH), 490 nm for lactate dehydrogenase (LDH), and at 532 and 600 nm for malondialdehyde (MDA).

Detection of ROS Content

The ROS levels were detected using a DCFH-DA fluorescent probe (Beyotime, Suzhou, China). DCFH-DA was diluted at a 1:1000 ratio in serum-free culture medium to a final concentration of 10 µmol/L and incubated with the cells for 20 minutes. The cells were washed three times with serum-free cell culture medium to thoroughly remove any excess probe that had not entered the cells. The cells were digested and resuspended in an appropriate volume of culture medium, transferred to a centrifuge tube, and then centrifuged at 1000 rpm for 5 minutes. Fluorescence detection was performed by flow cytometry within 30 minutes, using an excitation wavelength of 488 nm and an emission wavelength of 525 nm.

Western Blot Analysis

Western blot analysis was employed to assess the expression levels of Glutathione Peroxidase 4 (GPX4), Solute Carrier Family 7 Member 11 (SLC7A11), and Acyl-CoA Synthetase Long Chain Family Member 4 (ACSL4). For this purpose, total protein was isolated using RIPA lysis buffer (Beyotime, Suzhou, China), and its concentration was determined using a BCA kit (NCM Biotech, Suzhou, China). An equal amount of proteins (20 µg) was resolved using SDS-PAGE gel electrophoresis and subsequently transferred onto a PVDF membrane (Millipore, Burlington, MA, USA). The membrane was then blocked with 5% skim milk powder (BD, Franklin Lakes, NJ, USA) and incubated overnight at 4 °C with the following primary antibodies: anti-GPX4 antibody (Cat# ab125066, Abcam, Cambridge, UK, 1:1000), SLC7A11 polyclonal antibody (Cat# PA5-23082, Thermofisher, Waltham, MA, USA, 1:1000), anti-ACSL4 antibody (Cat# ab155282, Abcam, Cambridge, UK, 1:1000), and anti-GAPDH antibody (Cat# ab8245, Abcam, Cambridge, UK, 1:5000). The following day, after washing, the membrane was incubated with the appropriate HRP-conjugated secondary antibody, such as goat anti-mouse (Cat# bs-0296G-HRP, Bioss, Beijing, China, 1:5000) or goat anti-rabbit IgG H&L (Cat# bs-0295G-HRP, Bioss, Beijing, China, 1:5000), for one hour at room temperature. After that, protein bands were developed using a chemiluminescence imaging system (Tanon, Shanghai, China), and grayscale analysis was performed using Image J software.

Statistical Analysis

Experimental data were represented as mean ± standard error of the mean (SEM), and statistical analysis was conducted using GraphPad Prism 8 (Version 8.0.2, GraphPad Software Inc., San Diego, CA, USA). Multiple-group comparisons were performed using one-way ANOVA followed by Tukey's post hoc test to identify significant differences between groups. Comparison between two groups was conducted using the *t*-test. Statistical significance was set at a p-value of <0.05. All quantitative experiments were performed with three independent biological replicates (n = 3), unless otherwise specified.

Results

Cultivation and Identification of BMSCs

Initially, we verified the phenotype of BMSCs after the growth of cells reached 80% confluence. Flow cytometry analysis revealed that the proportion of CD44 and CD45 positive cells was 99.9% and 1.1%, respectively, which met the standard criteria for BMSCs surface antigens (Fig. 1A). Then, we evaluated the multidirectional differentiation potential of BMSCs. Alizarin red staining showed vivid red nodules, indicating calcium salt deposition within the cell clusters, serving as a visual marker of successful osteogenic differentiation (Fig. 1B). Oil Red O staining revealed distinct, red-stained intracellular lipid droplets, many appearing as spherical structures that aggregated into larger vesicles, which is a typical characteristic of adipogenic differentiation (Fig. 1C).

Additionally, Alcian blue staining showed a dense blue extracellular matrix within the cytoplasm of BMSCs, signifying successful chondrogenic induction characterized by glycosaminoglycan accumulation (Fig. 1D). These results confirmed that the BMSCs cell line had pluripotency towards adipogenesis, chondrogenesis, and osteogenesis, and met the established surface marker criteria for BMSCs. Therefore, the cell line was utilized in subsequent experimental research.

Mitochondria From BMSCs Could Be Transferred to Injured Endothelial Cells

To investigate whether healthy mitochondria from BMSCs can be transferred to injured endothelial cells, we first constructed an endothelial cell dysfunction model using HUVECs. HUVECs were exposed to medium containing 50 µg/mL ox-LDL and 100 µg/mL ox-LDL for 48 hours. We found that increasing ox-LDL concentrations substantially elevated the apoptosis rate of HUVECs (Fig. 2A). Furthermore, the levels of inflammatory factors, including IL-1β, IL-6, and TNF-α, also increased in a concentration-dependent manner in response to ox-LDL treatment (Fig. 2B). Additionally, the endothelial cell infiltration assay showed that the HUVECs permeability was significantly increased after ox-LDL treatment, especially

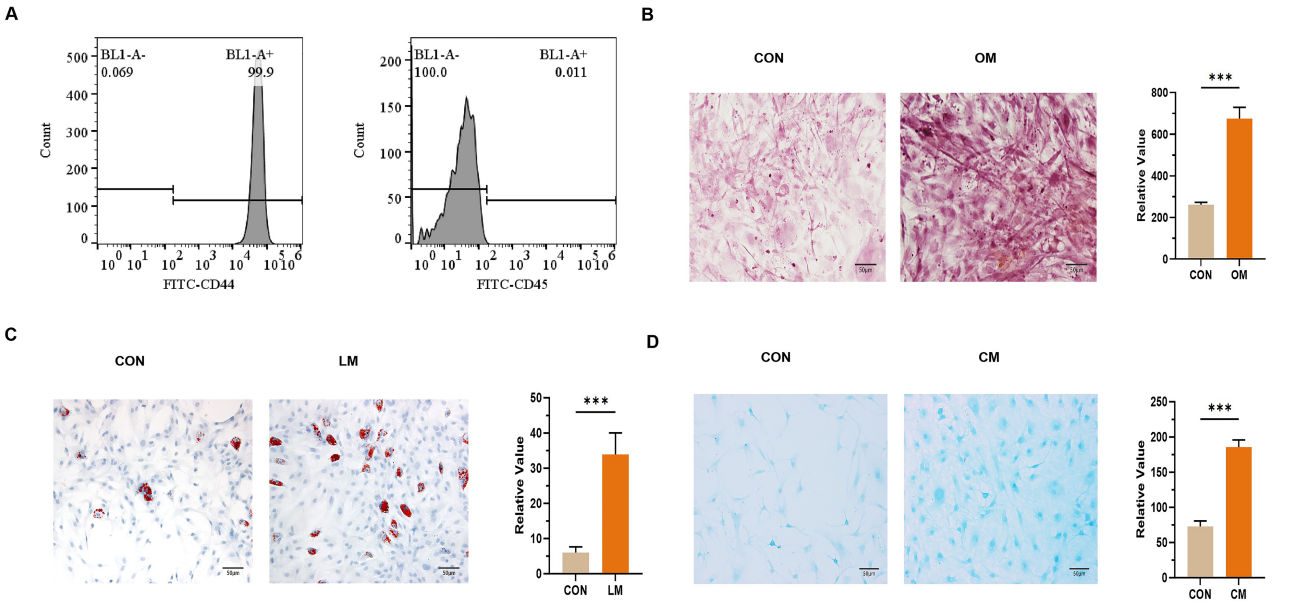

Fig. 1. Identification of bone marrow mesenchymal stem cells (BMSCs). (A) Flow cytometry for the expression of biomarkers in BMSCs. (B) Alizarin red staining for the intracellular calcium deposition and its quantitative analysis. Scale bar, 50 µm. For the osteogenic medium (OM) group, BMSCs were cultured using osteogenic induction medium after attachment. (C) Oil red O staining for assessing the number of intracellular lipid droplets and its quantitative analysis. Scale bar, 50 µm. For the lipogenic medium (LM) group, BMSCs were cultured using adipogenic induction medium after attachment. (D) Alcian blue staining for the identification of the chondrogenic differentiation ability of cells and its quantitative analysis. Scale bar, 50 µm. For chondrogenic medium (CM) group, BMSCs were cultured using chondrogenic induction medium after attachment. n = 3. CON, control group. ***$p < 0.001$ between indicated groups.

at 100 µg/mL (Fig. 2C). Based on these results, HUVECs treated with 100 µg/mL ox-LDL were used as endothelial cell injury models.

Furthermore, to explore whether mitochondria could be transferred to injured HUVECs through direct co-culture, BMSCs were pre-labeled with MitoTracker Red and HUVECs with MitoTracker Green, followed by co-culture for 24 hours. Laser confocal microscopy revealed distinct red fluorescent signals within the green-labeled HUVECs (Fig. 2D), confirming that mitochondria from BMSCs had successfully entered the recipient endothelial cells. This co-localization indicates active mitochondrial transfer rather than simple cell proximity. Furthermore, this mitochondrial uptake was accompanied by a significant increase in ATP levels and mitochondrial membrane potential ($p < 0.01$) (Fig. 2E–G), reinforcing the functional significance of this transfer. Collectively, these findings indicate that BMC-derived mitochondria can enter damaged endothelial cells and improve their ATP production.

Mitochondrial Transfer From BMSCs Improved Endothelial Cell Dysfunction

We evaluated whether mitochondrial transfer has a protective effect on injured HUVECs. Cell Counting Kit-8 (CCK-8) assay results showed that the viability of ox-LDL-treated HUVECs was significantly enhanced after co-cultivation with BMSCs ($p < 0.01$, Fig. 3A). Additionally, Transwell and wound healing assay revealed a substantial increase in the invasion and migration abilities of HUVECs in the presence of BMSCs ($p < 0.01$, Fig. 3B,C). Furthermore, flow cytometry analysis showed that co-culture with BMSCs substantially reduced the apoptosis rate of HUVECs (Fig. 3D). Moreover, the levels of inflammatory factors and cell permeability in HUVECs were also reduced following exposure to BMSCs ($p < 0.001$, Fig. 3E,F). Overall, these observations suggest that BMSCs may attenuate HUVEC injury through mitochondrial transfer.

Mitochondrial Transfer From BMSCs Inhibited Ferroptosis in Endothelial Cells

Given that excessive ROS production due to mitochondrial dysfunction is closely related to the induction of ferroptosis, we examined the impact of BMSCs on ferroptosis in HUVECs. Particularly, we assessed the impact of mitochondrial transfer of BMSCs on iron overload, ROS levels, and the expression of ferroptosis-related proteins in HUVECs. We found that co-culturing HUVECs with BMSCs significantly decreased the levels of Fe^{2+}, LDH, and MDA, while increasing GSH levels, indicating that BMSCs alleviated iron excess in HUVECs (Fig. 4A–D). Moreover, GSH levels in the HUVECs were significantly increased after co-culture with BMSCs ($p < 0.01$), suggesting enhanced

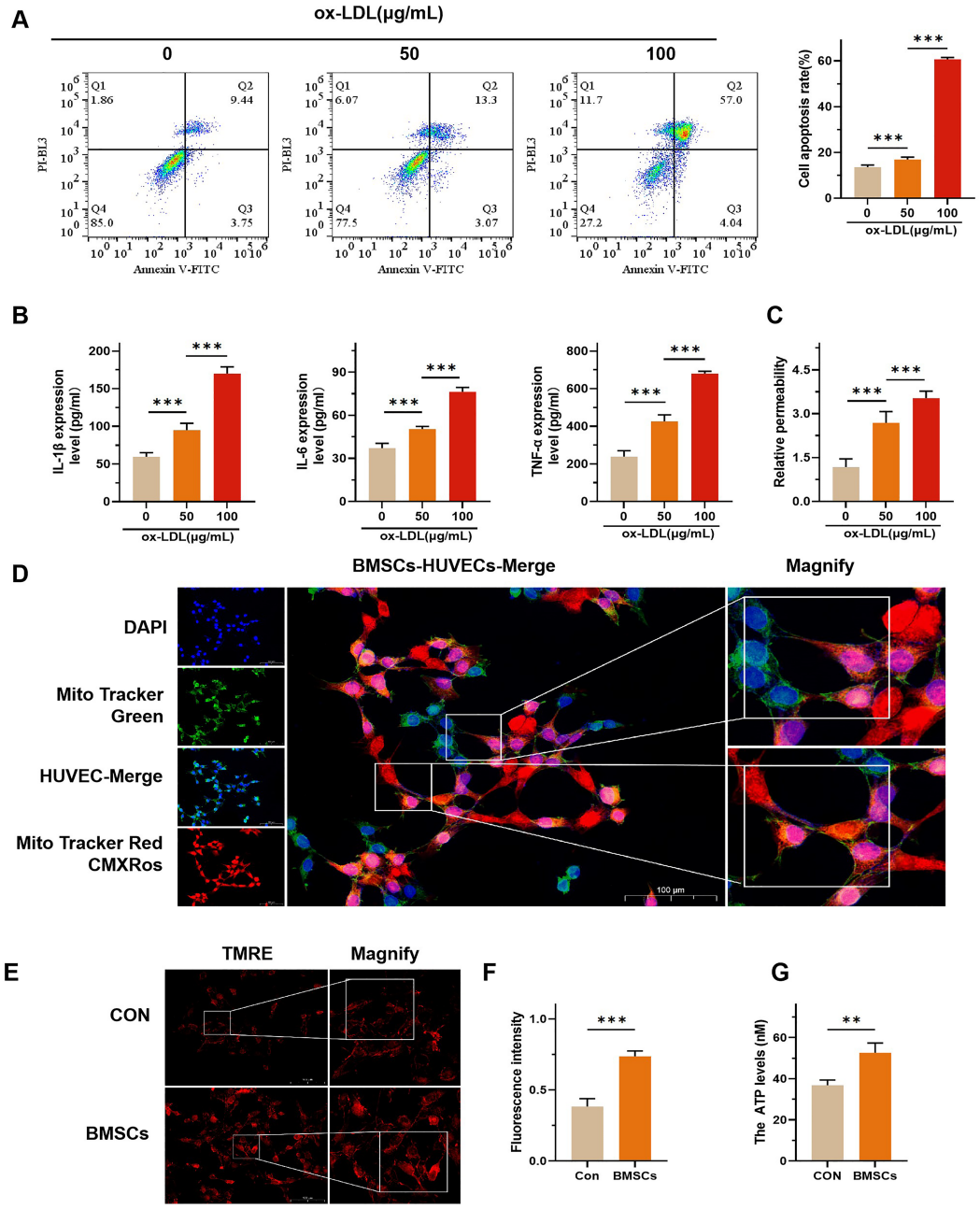

Fig. 2. Observing whether mitochondria could be transferred from BMSCs to endothelial cells. (A) Flow cytometry analysis to assess the apoptosis rate in human umbilical vein endothelial cells (HUVECs). HUVECs were treated with 50 or 100 μg/mL oxidized low-density lipoprotein (ox-LDL) for 48 hours. (B) The enzyme-linked immunosorbent assay (ELISA) assay to evaluate the expression levels of inflammatory factors. (C) Endothelial cell infiltration assay to examine endothelial cell function. (D) MitoTracker Red staining to observe mitochondrial metastasis after a co-culture with BMSCs and HUVECs treated with 100 μg/mL ox-LDL for 24 hours. Red indicated BMSCs pre-stained with MitoTracker Red, green indicated HUVECs pre-stained with MitoTracker Green, and blue indicated the nucleus of HUVECs. Scale bar, 100 μm. (E,F) Tetramethylrhodamine ethyl ester (TMRE) fluorescent analysis to examine mitochondrial membrane potential in HUVECs after co-cultivation and its quantitative analysis. Scale bar, 100 μm. (G) Detection of adenosine triphosphate (ATP) levels in HUVECs after co-cultivation. n = 3. $^{**}p < 0.01$ and $^{***}p < 0.001$ between indicated groups.

intracellular antioxidant capacity (Fig. 4B). Co-culture with BMSCs also reduced the ROS levels in HUVECs (Fig. 4E). Additionally, Western blot assay demonstrated that BMSCs upregulated the expression of the anti-ferroptosis proteins GPX4 and SLC7A11, while downregulating ACSL4 in HUVECs (Fig. 4F). Collectively, these findings indicate that BMSCs may prevent ferroptosis in HUVECs by providing healthy mitochondria.

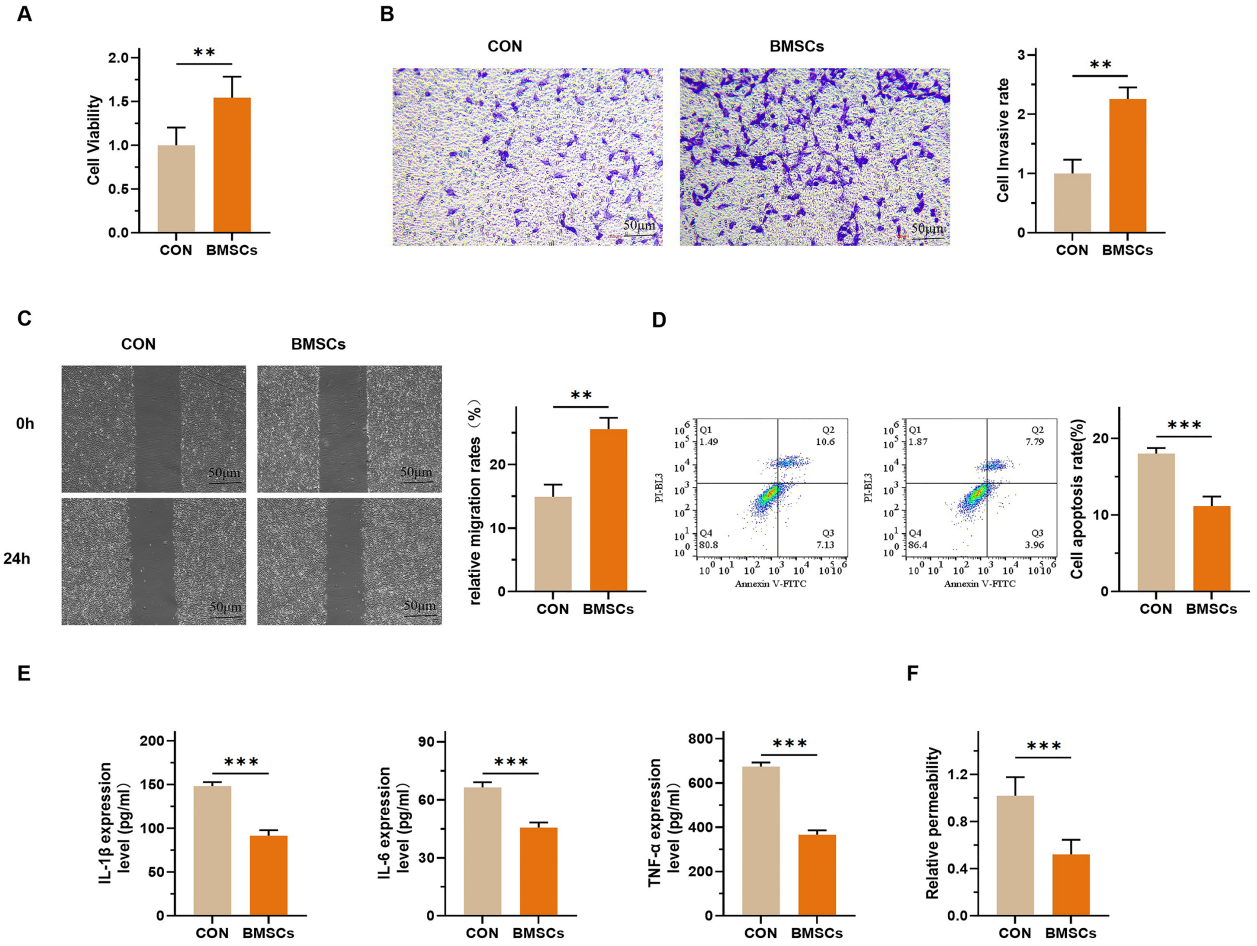

Fig. 3. The effect of mitochondrial transfer from BMSCs on endothelial cell dysfunction. (A) Cell Counting Kit-8 (CCK-8) assay to examine cell proliferation. (B) Transwell assay to assess cell invasion. Scale bar, 50 µm. (C) Wound healing assay to evaluate the migrating ability of cells at 24 hours. Scale bar, 50 µm. (D) Flow cytometry to detect the apoptosis rate of cells. (E) ELISA assay to examine the expression levels of inflammatory factors. (F) Endothelial cell infiltration assay to evaluate endothelial cell function. For the control (CON) group, HUVECs were treated with 100 µg/mL ox-LDL for 24 hours. For the BMSCs group, HUVECs treated with 100 µg/mL ox-LDL were co-cultured with BMSCs for 24 hours. n = 3. $^{**}p < 0.01$ and $^{***}p < 0.001$ between indicated groups.

Activation of Ferroptosis Reversed Endothelial Cell Injury Improved by BMSCs

Based on our results, we speculated that BMSCs may alleviate endothelial cell dysfunction by inhibiting ferroptosis. To test this hypothesis, the specific ferroptosis activator RSL3 was added to the co-culture system. The addition of RSL3 led to a decrease in the expression of anti-ferroptosis proteins and an increase in pro-ferroptosis proteins expression, indicating successful activation of ferroptosis (Fig. 5A). As expected, treatment with RSL3 significantly reduced the viability, invasion, and migration abilities of HUVECs in the co-culture system and substantially elevated HUVECs' apoptosis (Fig. 5B–E).

Before co-culture, ox-LDL-treated HUVECs showed elevated levels of inflammatory cytokines, including IL-1β, IL-6, and TNF-α, establishing a pro-inflammatory baseline.

After co-culture with BMSCs, these cytokine levels were significantly reduced ($p < 0.01$), indicating the anti-inflammatory potential of BMSCs under oxidative stress. However, treatment with the ferroptosis activator RSL3 reversed the suppressive effect of BMSCs, resulting in a rise in IL-1β, IL-6, and TNF-α levels, although the cytokines did not return to baseline levels. Additionally, RSL3 treatment elevated both inflammatory factor levels and cell permeability (Fig. 5F,G). These findings demonstrate that inhibiting ferroptosis is a crucial protective mechanism by which BMSC-derived mitochondrial transfer enhances endothelial cell function.

Discussion

Endothelial dysfunction is widely recognized as a key pathological driver in cardiovascular diseases, contributing to increased vascular permeability, chronic inflammation, and impaired vasodilation—all of which exacerbate the progression of atherosclerosis and thrombosis [17]. While

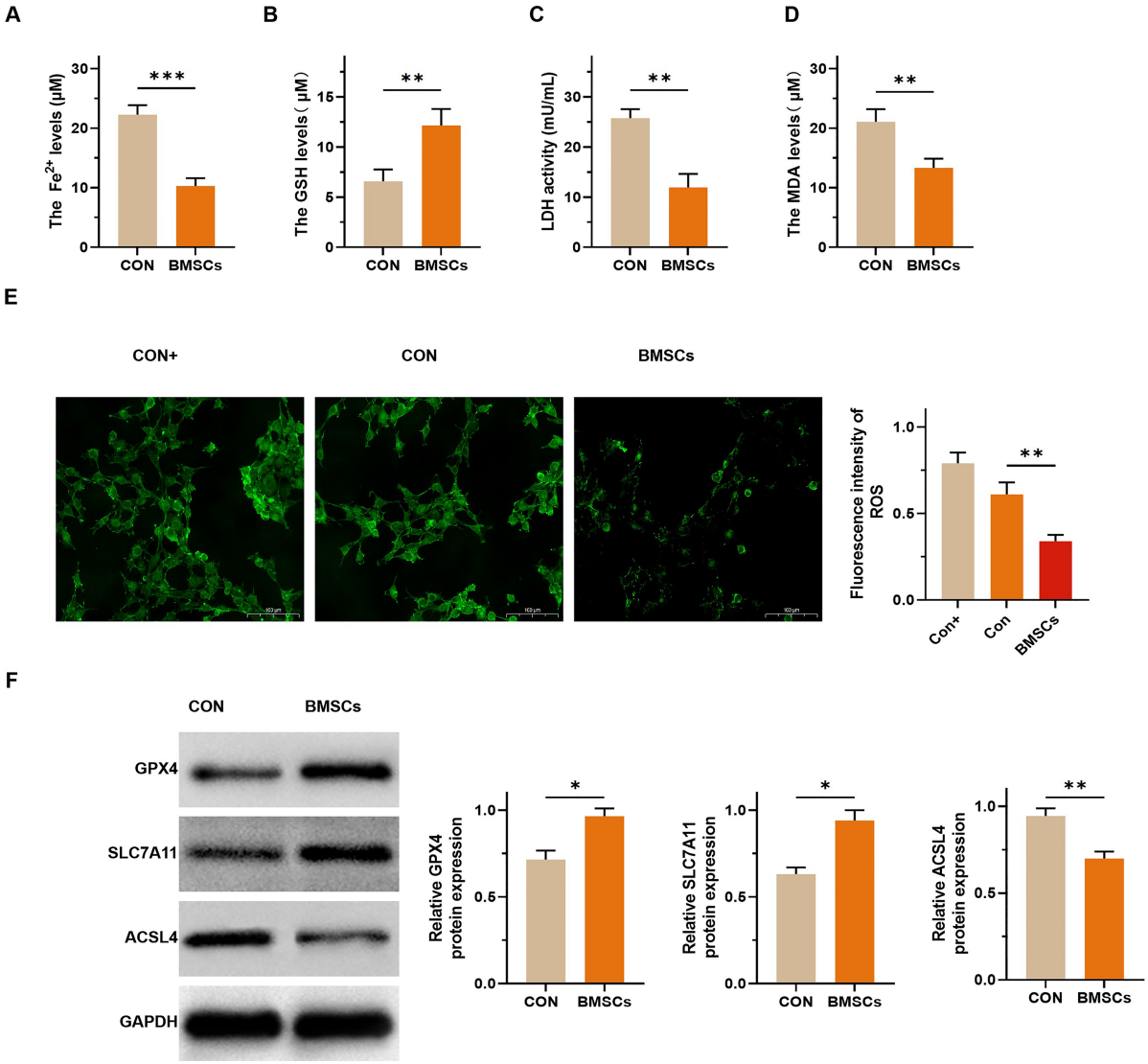

Fig. 4. The effect of mitochondrial transfer from BMSCs on ferroptosis in endothelial cells. (A) The levels of Fe^{2+} in HUVECs in the co-culture system. (B) The levels of glutathione (GSH) in HUVECs in the co-culture system. (C) The content of lactate dehydrogenase (LDH) in HUVECs in the co-culture system. (D) The content of malondialdehyde (MDA) in HUVECs in the co-culture system. (E) DCFH-DA fluorescent probe to detect ROS levels in different groups of HUVECs. 'CON+ group' indicates HUVECs treated with 10 μM CCCP as a positive control for ROS elevation; 'CON group' indicates untreated HUVECs; 'BMSCs group' refers to ox-LDL-injured HUVECs co-cultured with BMSCs for 24 hours. Scale bar, 100 μm. (F) Western blot assay to determine the expression levels of ferroptosis-related proteins, Glutathione Peroxidase 4 (GPX4), Solute Carrier Family 7 Member 11 (SLC7A11), and Acyl-CoA Synthetase Long Chain Family Member 4 (ACSL4). Glyceraldehyde-3-Phosphate Dehydrogenase (GAPDH) was used as a reference. n = 3. *$p < 0.05$, **$p < 0.01$ and ***$p < 0.001$ between indicated groups.

traditional perspectives have emphasized oxidative stress and cytokine imbalance as the major contributors, recent studies highlight the crucial role of mitochondrial dysfunction in modulating endothelial behavior. Although mitochondria are not the primary energy source for endothelial cells, they are pivotal for regulating cell migration, angiogenesis, and survival. Previous study has shown that impaired mitochondrial integrity increases ROS production and promotes endothelial injury [18]. However, relatively few studies have proposed directly restoring mitochondrial function in endothelial cells as a therapeutic strategy. Our findings provide novel mechanistic insight into this field by demonstrating that bone marrow mesenchymal stem cells (BMSCs) can restore endothelial function through mitochondrial transfer. Notably, we observed that mitochondrial donation from BMSCs significantly enhanced HUVEC viability, reduced permeability, and improved migratory capacity—all of which are key indicators of endothelial health and integrity.

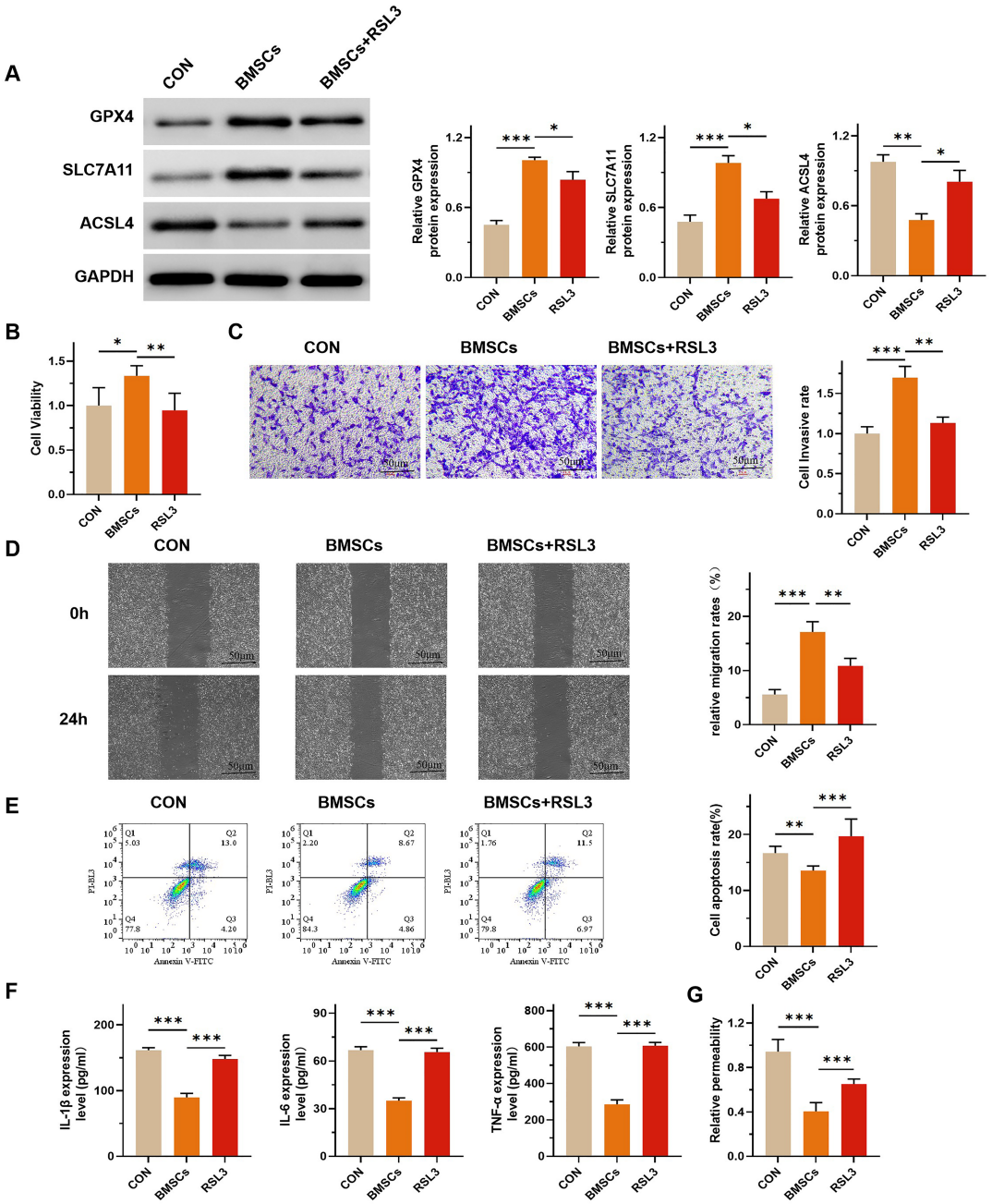

Fig. 5. Rescue experiments based on ferroptosis activators. (A) Western blot assay to assess the expression levels of ferroptosis-related proteins Glutathione Peroxidase 4 (GPX4), Solute Carrier Family 7 Member 11 (SLC7A11), and Acyl-CoA Synthetase Long Chain Family Member 4 (ACSL4). Glyceraldehyde-3-Phosphate Dehydrogenase (GAPDH) was used as a reference. (B) CCK-8 assay to examine cell proliferation ability. (C) Transwell assay to evaluate cell invasion ability. Scale bar, 50 µm. (D) Wound healing assay to assess the migration ability of cells at 24 hours. Scale bar, 50 µm. (E) Flow cytometry to detect the apoptosis rate of cells. (F) ELISA assay to determine the expression levels of inflammatory factors. (G) Endothelial cell infiltration assay to evaluate endothelial cell function. The CON and BMSCs groups underwent treatment as described above. The BMSCs+Rat Sarcoma Viral Oncogene Homolog (RAS)-selective lethal small molecule 3 (RSL3) group referred to HUVECs treated with 100 µg/mL ox-LDL and co-cultured with BMSCs, and 5 µmol/mL RSL3 was added. n = 3. *$p < 0.05$, **$p < 0.01$ and ***$p < 0.001$ between indicated groups.

Recent research has confirmed that BMSCs can transfer normal mitochondria to various damaged somatic cells, thereby enhancing their energy metabolism [11]. However, to the best of our knowledge, this study is the first to show that BMSC-mediated mitochondrial transfer exerts protective effects specifically by inhibiting ferropto-

sis in endothelial cells, revealing a novel anti-ferroptosis mechanism. Furthermore, unlike conventional ferroptosis interventions, which typically rely on small-molecule inhibitors such as ferrostatin-1 or upregulation of GPX4 expression [19], these approaches often neglect mitochondrial dysfunction, a key upstream factor in ferroptosis induction. Our results extend beyond these chemical strategies by demonstrating a biologically active, mitochondria-based protective mechanism. Consistent with previous reports demonstrating the regenerative capacity of BMSCs in repairing bone, cartilage, and adipose tissues [11], we confirmed their multipotency and verified their role in mitochondrial transfer through co-culture assays. After mitochondrial transfer, recipient HUVECs exhibited increased intracellular ATP levels and enhanced mitochondrial membrane potential, indicating the restoration of mitochondrial homeostasis and functional integrity.

Ferroptosis is a recently defined form of regulated cell death that is distinct from apoptosis and necrosis and is primarily driven by intracellular iron overload and subsequent lipid peroxidation [20]. Previous study has revealed that ferroptosis is closely associated with the pathogenesis of various diseases, including cardiovascular conditions, neurodegeneration, and cancers [21]. Mechanistically, disruption of intracellular iron metabolism can lead to excessive accumulation of Fe^{2+}, which catalyzes oxidative reactions and promotes the peroxidation of membrane lipids, ultimately resulting in cell death [22].

In line with these findings, our study also observed that endothelial cells subjected to oxidative stress exhibited elevated iron levels and clear ferroptosis-related phenotypes. However, unlike conventional approaches that utilize chemical inhibitors such as ferrostatin-1 or GPX4 overexpression to suppress ferroptosis, our findings demonstrate that mitochondrial transfer from BMSCs can exert a comparable inhibitory effect by restoring mitochondrial function and redox balance. Specifically, this transfer significantly improved intracellular energy status, reduced Fe^{2+} accumulation, and mitigated oxidative stress in injured HUVECs.

Furthermore, at the protein level, our findings support and extend previous reports regarding key regulators of ferroptosis. For instance, GPX4, a pivotal antioxidant enzyme, suppresses ferroptosis by neutralizing lipid peroxides [19]. SLC7A11, a component of the system Xc^- transporter, maintains glutathione synthesis by importing cystine, thereby contributing to redox homeostasis [23]. Conversely, ACSL4 promotes the synthesis of polyunsaturated phospholipids, which are substrates for lipid peroxidation and are essential for the execution of ferroptosis [24]. In our study, mitochondrial transfer led to upregulation of GPX4 and SLC7A11, along with downregulation of ACSL4, collectively providing molecular evidence that BMSCs can modulate canonical ferroptosis pathways via mitochondrial donation.

As demonstrated above, we confirmed that mitochondrial transfer from BMSCs to HUVECs inhibited ferroptosis in recipient cells. Based on this, we sought to assess whether the protective effect of BMSC-derived mitochondrial transfer on endothelial function relies on its ability to affect ferroptosis. For this purpose, we conducted rescue experiments using iron death-specific activators. Our results revealed that activation of ferroptosis reversed the protective impacts of mitochondrial transfer. Specifically, endothelial cells' survival, invasion, and migration abilities were reduced, the inflammatory response was intensified, and cellular permeability increased. Initially, co-culture with BMSCs reduced IL-1β, IL-6, and TNF-α levels in ox-LDL-injured HUVECs. However, the subsequent treatment with RSL3 reversed these effects, resulting in elevated inflammatory marker expression. These observations underscore the crucial role of BMSC-mediated mitochondrial transfer in inhibiting ferroptosis and improving endothelial cell function.

While these findings offer valuable preclinical insights, the current study was limited to the cellular level. For translational advancements of these results, we plan to assess the therapeutic efficacy of BMSC-mediated mitochondrial transfer in an *in vivo* atherosclerosis mouse model. Key endpoints will include changes in plaque area, endothelial permeability, and oxidative stress markers. The data will be crucial for determining the feasibility of applying this approach in cardiovascular regenerative therapies.

Despite the promising results, several limitations of this study should be acknowledged. First, although the ferroptosis activator RSL3 was applied to validate the role of mitochondrial transfer, a dedicated DMSO solvent control group was not included. Although the final DMSO concentration was maintained below 0.1%, which is generally non-toxic, future studies should include solvent controls to allow for more rigorous interpretation. Second, BMSC surface marker identification in this study was limited to CD44 and CD45. While these markers, together with successful tri-lineage differentiation, are commonly used indicators of mesenchymal stem cell identity, a more comprehensive characterization following International Society for Cellular Therapy (ISCT) guidelines (including markers CD73, CD90, and CD105) was not conducted due to technical constraints and should be addressed in future studies. Third, although multipotent differentiation of BMSCs was confirmed using standard staining protocols, representative images and quantitative analyses were not included in this version of the study. Moreover, we cannot fully exclude the influence of BMSC-secreted factors beyond mitochondria, such as cytokines or exosomes. The specificity of Mito-Tracker staining also carries limitations, such as potential dye leakage or non-specific uptake. These aspects should be addressed in future investigations to further validate the identity and functional role of BMSC.

In summary, our study reveals that BMSCs protect injured HUVECs by transferring mitochondria, thereby suppressing ferroptosis and enhancing endothelial function. Our findings provide a strong correlation between ferroptosis and endothelial function, offering an important theoretical basis for developing targeted diagnostic and therapeutic approaches for cardiovascular diseases, especially atherosclerosis. This work not only expands our understanding of ferroptosis regulation but also highlights mitochondrial donation as a novel therapeutic strategy. Unlike conventional chemical inhibitors, this approach utilizes a naturally occurring cellular process to restore endothelial resilience, providing a potentially more adaptable and sustainable option for clinical applications. Overall, this study offers a new perspective into the therapeutic potential of bone marrow mesenchymal stem cells and lays a theoretical foundation for developing innovative cell-based therapeutic strategies.

Conclusion

In this study, we demonstrated that bone marrow mesenchymal stem cells (BMSCs) can transfer functional mitochondria to endothelial cells, significantly improving their viability and mitigating the detrimental effects of ferroptosis. Mitochondrial transfer from BMSCs enhances endothelial cell function by reducing iron accumulation, oxidative stress, and lipid peroxidation, key contributors to ferroptosis. Furthermore, inhibiting ferroptosis through mitochondrial donation represents a promising therapeutic strategy for addressing endothelial dysfunction and atherosclerosis. These findings offer new insights into the potential of BMSCs in treating cardiovascular diseases, providing a foundation for future *in vivo* studies to further validate their therapeutic efficacy.

Availability of Data and Materials

The data used to support the findings of this study are available from the corresponding author upon request.

Author Contributions

GKW: Conceptualization; Methodology; Data curation; Formal analysis; Writing - Original draft; Writing - Review & Editing. SQL: Conceptualization; Methodology; Project administration; Writing - Review & Editing. FL: Resources; Statistic analysis; Visualization; Writing - Review & Editing. ZGZ: Conceptualization; Methodology; Supervision; Writing - Review & Editing. All authors read and approved the final version of the manuscript. All authors have participated sufficiently in the work and agreed to be accountable for all aspects of the work.

Ethics Approval and Consent to Participate

Not applicable.

Acknowledgment

Not applicable.

Funding

This research received no external funding.

Conflict of Interest

The authors declare no conflict of interest.

References

[1] Fan B, Niu Y, Ren Z, Wei S, Ma Y, Su J, *et al*. Long Noncoding RNA MMP2-AS1 Contributes to Progression of Renal Cell Carcinoma by Modulating miR-34c-5p/MMP2 Axis. Journal of Oncology. 2022; 2022: 7346460. https://doi.org/10.1155/2022/7346460.

[2] Song P, Fang Z, Wang H, Cai Y, Rahimi K, Zhu Y, *et al*. Global and regional prevalence, burden, and risk factors for carotid atherosclerosis: a systematic review, meta-analysis, and modelling study. The Lancet. Global Health. 2020; 8: e721–e729. https://doi.org/10.1016/S2214-109X(20)30117-0.

[3] d'Aiello A, Filomia S, Brecciaroli M, Sanna T, Pedicino D, Liuzzo G. Targeting Inflammatory Pathways in Atherosclerosis: Exploring New Opportunities for Treatment. Current Atherosclerosis Reports. 2024; 26: 707–719. https://doi.org/10.1007/s11883-024-01241-3.

[4] Yang DR, Wang MY, Zhang CL, Wang Y. Endothelial dysfunction in vascular complications of diabetes: a comprehensive review of mechanisms and implications. Frontiers in Endocrinology. 2024; 15: 1359255. https://doi.org/10.3389/fendo.2024.1359255.

[5] Gimbrone MA, Jr, García-Cardeña G. Endothelial Cell Dysfunction and the Pathobiology of Atherosclerosis. Circulation Research. 2016; 118: 620–636. https://doi.org/10.1161/CIRCRESAHA.115.306301.

[6] Cornelissen A, Guo L, Sakamoto A, Virmani R, Finn AV. New insights into the role of iron in inflammation and atherosclerosis. EBioMedicine. 2019; 47: 598–606. https://doi.org/10.1016/j.ebiom.2019.08.014.

[7] Zhang H, Zhou S, Sun M, Hua M, Liu Z, Mu G, *et al*. Ferroptosis of Endothelial Cells in Vascular Diseases. Nutrients. 2022; 14: 4506. https://doi.org/10.3390/nu14214506.

[8] Bai T, Li M, Liu Y, Qiao Z, Wang Z. Inhibition of ferroptosis alleviates atherosclerosis through attenuating lipid peroxidation and endothelial dysfunction in mouse aortic endothelial cell. Free Radical Biology & Medicine. 2020; 160: 92–102. https://doi.org/10.1016/j.freeradbiomed.2020.07.026.

[9] Li J, Jia YC, Ding YX, Bai J, Cao F, Li F. The crosstalk between ferroptosis and mitochondrial dynamic regulatory networks. International Journal of Biological Sciences. 2023; 19: 2756–2771. https://doi.org/10.7150/ijbs.83348.

[10] Qu K, Yan F, Qin X, Zhang K, He W, Dong M, *et al*. Mitochondrial dysfunction in vascular endothelial cells and its role in atherosclerosis. Frontiers in Physiology. 2022; 13: 1084604. https://doi.org/10.3389/fphys.2022.1084604.

[11] Zhang F, Zheng X, Zhao F, Li L, Ren Y, Li L, *et al*. TFAM-Mediated mitochondrial transfer of MSCs improved the perme-

ability barrier in sepsis-associated acute lung injury. Apoptosis: an International Journal on Programmed Cell Death. 2023; 28: 1048–1059. https://doi.org/10.1007/s10495-023-01847-z.

[12] Paliwal S, Chaudhuri R, Agrawal A, Mohanty S. Regenerative abilities of mesenchymal stem cells through mitochondrial transfer. Journal of Biomedical Science. 2018; 25: 31. https://doi.org/10.1186/s12929-018-0429-1.

[13] Prajapat SK, Maharana KC, Singh S. Mitochondrial dysfunction in the pathogenesis of endothelial dysfunction. Molecular and Cellular Biochemistry. 2024; 479: 1999–2016. https://doi.org/10.1007/s11010-023-04835-8.

[14] Liu D, Gao Y, Liu J, Huang Y, Yin J, Feng Y, *et al*. Intercellular mitochondrial transfer as a means of tissue revitalization. Signal Transduction and Targeted Therapy. 2021; 6: 65. https://doi.org/10.1038/s41392-020-00440-z.

[15] Li H, Wang C, He T, Zhao T, Chen YY, Shen YL, *et al*. Mitochondrial Transfer from Bone Marrow Mesenchymal Stem Cells to Motor Neurons in Spinal Cord Injury Rats via Gap Junction. Theranostics. 2019; 9: 2017–2035. https://doi.org/10.7150/thno.29400.

[16] Wang K, Zhou L, Mao H, Liu J, Chen Z, Zhang L. Intercellular mitochondrial transfer alleviates pyroptosis in dental pulp damage. Cell Proliferation. 2023; 56: e13442. https://doi.org/10.1111/cpr.13442.

[17] Xu S, Ilyas I, Little PJ, Li H, Kamato D, Zheng X, *et al*. Endothelial Dysfunction in Atherosclerotic Cardiovascular Diseases and Beyond: From Mechanism to Pharmacotherapies. Pharmacological Reviews. 2021; 73: 924–967. https://doi.org/10.1124/pharmrev.120.000096.

[18] Luo Z, Yao J, Wang Z, Xu J. Mitochondria in endothelial cells angiogenesis and function: current understanding and future perspectives. Journal of Translational Medicine. 2023; 21: 441. https://doi.org/10.1186/s12967-023-04286-1.

[19] Seibt TM, Proneth B, Conrad M. Role of GPX4 in ferroptosis and its pharmacological implication. Free Radical Biology & Medicine. 2019; 133: 144–152. https://doi.org/10.1016/j.freeradbiomed.2018.09.014.

[20] Mou Y, Wang J, Wu J, He D, Zhang C, Duan C, *et al*. Ferroptosis, a new form of cell death: opportunities and challenges in cancer. Journal of Hematology & Oncology. 2019; 12: 34. https://doi.org/10.1186/s13045-019-0720-y.

[21] Jiang X, Stockwell BR, Conrad M. Ferroptosis: mechanisms, biology and role in disease. Nature Reviews. Molecular Cell Biology. 2021; 22: 266–282. https://doi.org/10.1038/s41580-020-00324-8.

[22] Liu J, Kang R, Tang D. Signaling pathways and defense mechanisms of ferroptosis. The FEBS Journal. 2022; 289: 7038–7050. https://doi.org/10.1111/febs.16059.

[23] Koppula P, Zhuang L, Gan B. Cystine transporter SLC7A11/xCT in cancer: ferroptosis, nutrient dependency, and cancer therapy. Protein & Cell. 2021; 12: 599–620. https://doi.org/10.1007/s13238-020-00789-5.

[24] Doll S, Proneth B, Tyurina YY, Panzilius E, Kobayashi S, Ingold I, *et al*. ACSL4 dictates ferroptosis sensitivity by shaping cellular lipid composition. Nature Chemical Biology. 2017; 13: 91–98. https://doi.org/10.1038/nchembio.2239.